JEE Journal of Ecological Engineering

Journal of Ecological Engineering, 2027, 28(1), 172–182
https://doi.org/10.12911/22998993/240484
ISSN 2299–8993, License CC-BY 4.0

Received: 2026.08.26
Accepted: 2026.11.16
Published: 2026.12.01

Wind-induced energy harvesting via an aeroelastic resonator with a dual flexible beam: Effect of magnetic coupling

Tomasz Haniszewski[1], Jerzy Margielewicz[1], Damian Gaska[1], Jacek Caban[2], Grzegorz Litak[2]

[1] Faculty of Transport and Aviation Engineering, Silesian University of Technology, ul. Krasińskiego 8, 40-019 Katowice, Poland
[2] Faculty of Mechanical Engineering, Lublin University of Technology, ul. Nadbystrzycka 36, 20-618 Lublin, Poland
* Corresponding author's e-mail: j.caban@pollub.pl

ABSTRACT

This paper investigates an ambient energy harvesting system operating under specific airflow velocities, utilizing two flexible cantilever beams terminated with cylinders and equipped with piezoelectric transducers. The system vibrations are induced by the vortex shedding phenomenon, modelled as a Van der Pol oscillator. The analysis covers both repulsive and attractive magnetic configurations. Specifically, the impact of the cylinder diameter and the body mass ratio μ on the generated voltage and broadband performance was examined. The results indicate that increasing the cylinder diameter expands the flow velocity range in which the moderate output voltage is achieved, reaching values up to 25 V. The application of an asymmetric mass ratio (μ = 0.5) further enhances the system's bandwidth, enabling effective operation across a range from 1 to 14 m/s. Optimal performance was observed for a 0.12 m diameter cylinder in an attractive configuration with μ = 0.5, where the peak power output reached approximately 800 μW. This study confirms that by optimizing the magnetic configuration and geometric parameters, it is possible to significantly increase the efficiency of Vortex-Induced Vibration (VIV) energy harvesters utilizing piezoelectric transducers and magnetic interactions.

Keywords: energy harvesting system; piezoelectric; flow structure interaction; vortex induced vibration; magnetic interaction.

INTRODUCTION

Vibration energy harvesting has emerged as a crucial promising technology for powering small-scale electronic devices by scavenging wasted energy from the environment. Although the amount of energy captured is relatively low, it is sufficient to power wireless sensors and data transmission modules, enabling the creation of self-sustaining monitoring systems and allowing batteries to be recharged, thereby extending their operational lifetime (Ahmed et al., 2026; Jing et al., 2025; Liu et al., 2026; Su et al., 2025; Ullah et al., 2025; Yang et al., 2018; Zhang et al., 2026). These devices are particularly well-suited for integration into transportation and industrial infrastructure, such as bridges and pipelines, where traditional power supply with wires and replaced batteries may be impractical or costly (Gazkooh et al., 2025). Harvesting kinetic energy from ambient vibrations offers a convenient means of stabilising the environment through conversion to electrical power (Shehu et al., 2024; Ullah et al., 2025). Among the various strategies, harvesting kinetic energy from wind flow is one possible approach (Ahmed et al., 2026; Liu et al., 2026; Su et al., 2025). In such a system a bluff body, mechanical oscillator and electro-mechanical transducer are designed to absorb, firstly, mechanical energy from the wind flow in the mechanical structure and than transform into the electrical power (Ma & Zhou 2022; Wang et al., 2020). Therefore, the

leading mechanisms to absorb the wind energy into the mechanical oscillator equipped with the bluff body exposed to vortex induced vibrations (VIV), galloping and wake oscillations (Litak et al., 2025). The captured mechanical energy is transformed by piezoelectric transducers or by other multi-physics device (including electromagnetic (Borowiec et al., 2026; Zhang et al., 2025), triboelectric (Zhou et al., 2024)) working in the linear coupling with the oscillator. If the bluff-bodies are of the cylindrical shape and the wind velocity field has uniform distribution, the VIV mechanism is the most effective (Facchinetti et al., 2004; Litak et al., 2025; Wang et al., 2020). This scenario exploits the internal resonance between the mechanical and flow modes. Simply, the vortex interaction with the mechanical structure via creation and shedding synchronizes usually with the first mode of cantilever spring and mass oscillator. Sweeping the wind speed one notice increase and decrease of the oscillation amplitude. Due to fluctuations in wind speed one can expect differences in the frequency of excitation of the mechanical structure and finally for a linear device drop in vibration amplitude and consequently in power output. To overcome this deficiency nonlinearities are introduced to the mechanical oscillator by including impacts, magnetic field or some geometrical nonlinearities (Cottone et al., 2009; Erturk et al., 2009; Litak et al., 2010; Maity et al., 2026; Margielewicz et al., 2022; Yang et al., 2023). Vibration energy harvesting is based on the ambient vibration sources which energy could be dissipated in other way. These are distributed energy sources and the limitations of volume and mass of the desired harvesters which provide challenges to improve the effectives and design the smaller size (miniaturized) device coupled in pairs or arrays. In the present paper we are following that way. In our mechanical structure we include two parallel oscillators coupled by magnetic field. This nonlinear coupling is an extension of the experimental work (Ma et al., 2024) but also distinguish our approach from the linear made the spring connection (Maity et al., 2026a) and the interaction through the vortices (Sadasivan et al., 2025). Using simple assumption on the magnets interaction and reduced model for vortex interactions. To convert mechanical energy piezoelectric transducers are used. The main novelty of this work lies in the synergistic integration of an asymmetric mass ratio $\mu = 0.5$ combined with a nonlinear attractive magnetic configuration. Unlike traditional symmetric or linearly coupled systems, this specific configuration breaks structural symmetry, triggering a mutual synchronization that dramatically lowers the cut-in wind velocity to 1 m/s and expands the operational bandwidth across the entire 1–14 m/s range.

MATHEMATICAL MODEL

The subject of the model research in this case (Fig. 1a) is an energy harvesting system consisting of a rigid body as the frame (*V*) and two flexible cantilever beams (*III*). Piezoelectric transducers (*IV*), responsible for converting mechanical energy into electrical energy, are coupled to the beams. As a result of elastic deformation of the

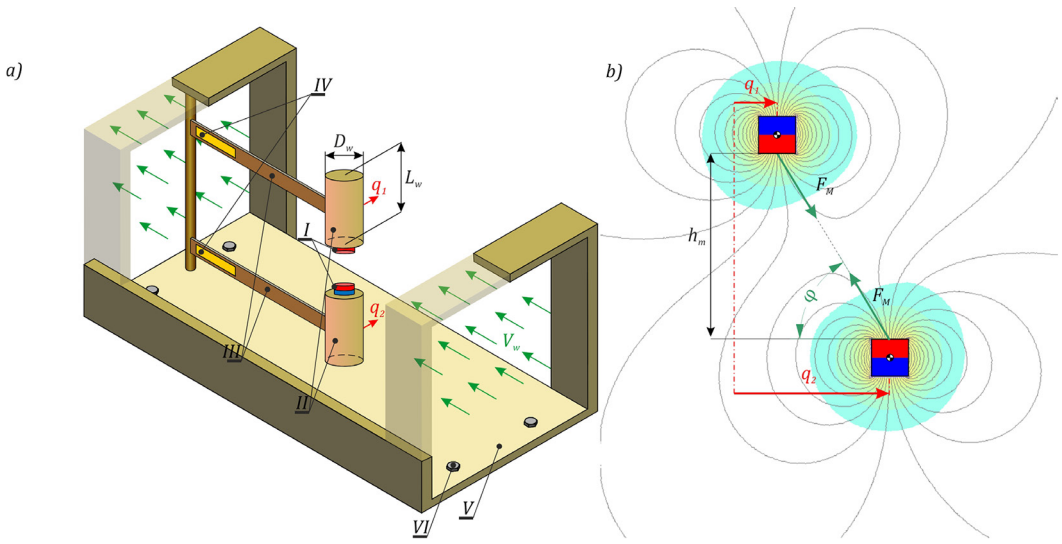

Figure 1. (a) Schematic of aeroelastic resonator with a dual flexible beam model, (b) magnets interaction

beams, piezoelectric patches change their polarization. The induced charge on the piezoelectric electrodes can simultaneously be used to power external electrical devices, with the electrode terminals connected to a load resistor of value R_l. The movement of the system is induced by airflow at a specific velocity V_w, ranging from 1 to 14 m/s. The body (*V*) is fixed to the base by means of bolts (*VI*). The investigated system comprises two flexible cantilever beams equipped with cylinders (*II*) at their ends, which induce lateral vibrations under the influence of the airflow, and mediated by magnets (*I*). A distinctive feature of the proposed design is the ability to influence the energy harvesting capacity by changing the polarization of the interacting magnetic poles (Fig. 1(b)).

In the present work, the primary focus is on the voltage signal on the resistor generated by each of the piezoelectric elements and the influence of the wind speed variation (within the range of 1–14 m/s) and the magnetic polarization on the voltage output. The formal basis for evaluating the energy and dynamic properties of the studied design is a mathematical model (1). Its dimensional representation is expressed by a system of six differential equations, which are presented in Equation 1.

These formulas are based on work (Litak et al., 2025), where a single oscillator was investigated. Here system of equations in its basic form consists of three doubled equations for the two beams. The first and third equations (1) account for the dynamics of the mechanical part, i.e., the beam with the cylinder, while the second and fourth represent the vortex-generating system based on the Van der Pol equation suggested by (Facchinetti et al., 20204; Litak et al., 2025). The equations are coupled with each other and with the fifth and sixth equations, which cover the electrical part including the load, forming three pairs. The primary variables include the lateral vibrations of the elastic beams, represented by the generalized displacement variables q_1, q_2, while the voltage output is expressed by the variables u_1, u_2, respectively. The geometry of the investigated system is defined by the cylinder diameter D_W and its height L_W. The parameters shaping the characteristics of the cantilever beam are defined by C_B, b, and m, representing stiffness, damping, and mass. Regarding the excitation, the wind speed is determined by the parameter V_w and ρ (air density). Accordingly, the parameters C_l and C_d define the lift and drag coefficients. The coefficients A_e and β are responsible for the operation of the vortex generator and are referred to as the empirical matching parameters (Litak et al., 2025). The vortex shedding frequency is defined by the parameter ω_s. The electrical circuit connects the mechanical and electrical parts through the electromechanical coupling coefficient θ.

In the proposed design of the energy harvesting system, the nonlinearity is determined by the interacting magnetic poles and the vortex generator in the form of the Van der Pol equation. The corresponding relationships (2), as seen from the perspective of the inertial elements m_1, m_2, can be written as the following equations:

$$\begin{aligned} F_1 &= F_{B1} \pm F_M \\ F_2 &= F_{B2} \pm F_M \end{aligned} \tag{2}$$

where: the terms F_{Bi} = 1, 2 denote the restore force of each of springs while F_M states for the magnetic force.

$$\begin{cases} m_1\dfrac{d^2q_1}{dt^2} + b_1\dfrac{dq_1}{dt} + c_{B1}q_1 - F_M + k_p u_1 = \dfrac{1}{4}\rho V_w^2 D_w L_w C_l z_1 - \dfrac{1}{2}\rho V_w D_w L_w C_d \dfrac{dq_1}{dt} \\ \dfrac{d^2z_1}{dt^2} + \beta\omega_s(z_1^2 - 1)\dfrac{dz_1}{dt} + \omega_s^2 z_1 = \dfrac{A_e}{D_w}\dfrac{d^2q_1}{dt^2} \\ m_2\dfrac{d^2q_2}{dt^2} + b_2\dfrac{dq_2}{dt} + c_{B2}q_2 + F_M + k_p u_2 = \dfrac{1}{4}\rho V_w^2 D_w L_w C_l z_2 - \dfrac{1}{2}\rho V_w D_w L_w C_d \dfrac{dq_2}{dt} \\ \dfrac{d^2z_2}{dt^2} + \beta\omega_s(z_2^2 - 1)\dfrac{dz_2}{dt} + \omega_s^2 z_2 = \dfrac{A_e}{D_w}\dfrac{d^2q_2}{dt^2} \\ C_p\dfrac{du_1}{dt} + \dfrac{1}{R_l}u_1 - k_p\dfrac{dq_1}{dt} = 0 \\ C_p\dfrac{du_2}{dt} + \dfrac{1}{R_l}u_2 - k_p\dfrac{dq_2}{dt} = 0 \end{cases} \tag{1}$$

Using a simple approximation of magnets much larger in size then their relative distance, the magnetic interaction force is inversely proportional to the square of the distance r_m measured between the poles. The polarization of the interacting poles is established using the "±" sign. In the case of a repulsive configuration, the sign coefficient q_m is assigned a negative sign ("-"). Conversely, for an attractive configuration, these values are positive. The following equations (3, 4), which represent the forces acting on individual inertial elements, were derived with reference to the configuration shown in Figure 1b using r_m precise approximation according to Ref (Sang et al., 2026). This leads to an explicit representation of the resulting mechanical characteristics of the investigated energy harvesting system design:

$$\begin{gathered} F_1 = c_{B1}q_1 - \frac{q_m(q_1-q_2)}{\left(\sqrt{h_m^2+(q_1-q_2)^2}\right)^3} \\ F_2 = c_{B2}q_2 + \frac{q_m(q_1-q_2)}{\left(\sqrt{h_m^2+(q_1-q_2)^2}\right)^3} \\ r_m = \sqrt{h_m^2+(q_1-q_2)^2}, \quad cos(\varphi) = \frac{q_1-q_2}{\sqrt{h_m^2+(q_1-q_2)^2}}, \end{gathered} \tag{3}$$

The magnetic force is equal to:

$$F_M = \frac{q_m(q_1-q_2)}{\left(\sqrt{h_m^2+(q_1-q_2)^2}\right)^3} \tag{4}$$

where: $q_m = f_m h^2{}_m$.

The mathematical model derived in this manner is subsequently transformed into a dimensionless form (5). This approach is justified as it significantly reduces simulation time and allows for the use of much smaller numerical values, thereby minimizing the impact of rounding errors associated with floating-point calculations. From the perspective of the energy harvesting system's design, the following assumptions were made: $c_{B1} = c_{B2}$, $b_1 = b_2$, and $m_1 = m_2$. Incorporating these assumptions and performing several elementary transformations leads to the dimensionless representation of the mathematical model:

$$\begin{gathered} \ddot{\chi}_1 + \delta\dot{\chi}_1 + \chi_1 - Q\frac{(\chi_1-\chi_2)}{\left(\sqrt{(\chi_1-\chi_2)^2+1^2}\right)^3} + \theta U_1 = \\ = F_1\omega^2 Z_1 - F_2\omega\dot{\chi}_1 \\ \mu\ddot{\chi}_2 + \delta\dot{\chi}_2 + \chi_2 + Q\frac{(\chi_1-\chi_2)}{\left(\sqrt{(\chi_1-\chi_2)^2+1^2}\right)^3} + \theta U_2 = \\ = F_1\omega^2 Z_2 - F_2\omega\dot{\chi}_2 \\ \ddot{Z}_1 + \beta\eta(Z_1^2-1)\dot{Z}_1 + \eta^2 Z_1 = W\ddot{\chi}_1 \\ \ddot{Z}_2 + \beta\eta(Z_2^2-1)\dot{Z}_2 + \eta^2 Z_2 = W\ddot{\chi}_2 \\ \dot{U}_1 + \kappa U_1 - \dot{\chi}_1 = 0 \\ \dot{U}_2 + \kappa U_2 - \dot{\chi}_2 = 0 \end{gathered} \tag{5}$$

Table 1. Geometric and physical parameters characterizing the investigated system

Parameter	Symbol	Value	Unit
Cantilever beam load (mass)	m_1, m_2	0.0078	kg
Total energy loss coefficient	b_1, b_2	0.003	Nsm^{-1}
Cantilever beam stiffness	CB_1, CB_2	26	Nm^{-1}
Cantilever beam stiffness	ρ	1.2041	kgm^{-3}
Vortex shedding frequency	ω_s	$2\pi S_t V_w D_w{}^{-1}$	s^{-1}
Strouhal number	S_t	0.2	-
Lift coefficient	C_l	0.3	-
Drag coefficient	C_d	1.2	-
Empirical matching parameters	A_e	12	-
	β	0.24	-
Cylinder diameter	D_w	0.03, 0.06, 0.09	m
Cylinder height	L_w	0.09	m
Distance between magnets	h_m	0.02	m
Magnetic attraction force (max capacity)	f_m	50	N
Load resistance	R_l	10^6	Ω
Piezoelectric capacitance	C_p	100	nF
Piezoelectric constant	k_p	$2{\cdot}10^{-5}$	NV^{-1}

where:

$$\mu = \frac{m_2}{m_1}, \quad Q = \frac{q_m}{h_m^3 \omega_0^2 m_1}, \quad \eta = \frac{\omega_s}{\omega_0}, \quad \omega_0^2 = \frac{c_B}{m_1}, \quad \tau = \omega_0 t, \quad \delta = \frac{b}{m_1 \omega_0}, \quad \omega = \frac{V_W}{\omega_0},$$
$$\chi_1 = \frac{q_1}{h_m}, \quad \chi_2 = \frac{q_2}{h_m}, \quad W = \frac{A_e h_m}{D_w}, \quad F_1 = \frac{1}{4}\frac{\rho D_w L_w C_l}{h_m m_1}, \quad F_2 = \frac{1}{2}\frac{\rho D_w L_w C_d}{m_1},$$
$$U_1 = \frac{C_P}{k_P h} u_1, \quad U_2 = \frac{C_P}{k_P h} u_2, \quad \theta = \frac{k_p^2}{C_p \omega_0^2 m_1}, \quad \kappa = \frac{1}{C_p \omega_0 R_l}.$$

The derived mathematical model of the investigated energy harvesting system design serves as a formal basis for conducting quantitative and qualitative computer simulations. All subsequent numerical experiments were conducted based on the physical and geometric parameter values summarized in Table 1.

EFFECT OF BLUFF BODY DIAMETER AND BODY MASS RATIO μ

The calculations presented below were performed for a small initial displacement of one of the beams from its equilibrium position. The objective was to perturb the system from its stable state, thereby initiating disturbances and vortex shedding. Specifically, the beam described by the generalized coordinate q_1 was initially excited, while the second beam was excited through magnetic coupling in both attractive and repulsive configurations. The computations were carried out using Wolfram Mathematica software with an automatic integration step. The computational procedure was divided into two groups of data: the influence of the cylinder diameter and the influence of the body mass ratio μ.

Based on the performed simulations, it can be concluded that a larger diameter (at a constant mass, as per our assumption) contributes to enhanced system efficiency under varying wind speed conditions. The wide range of flow

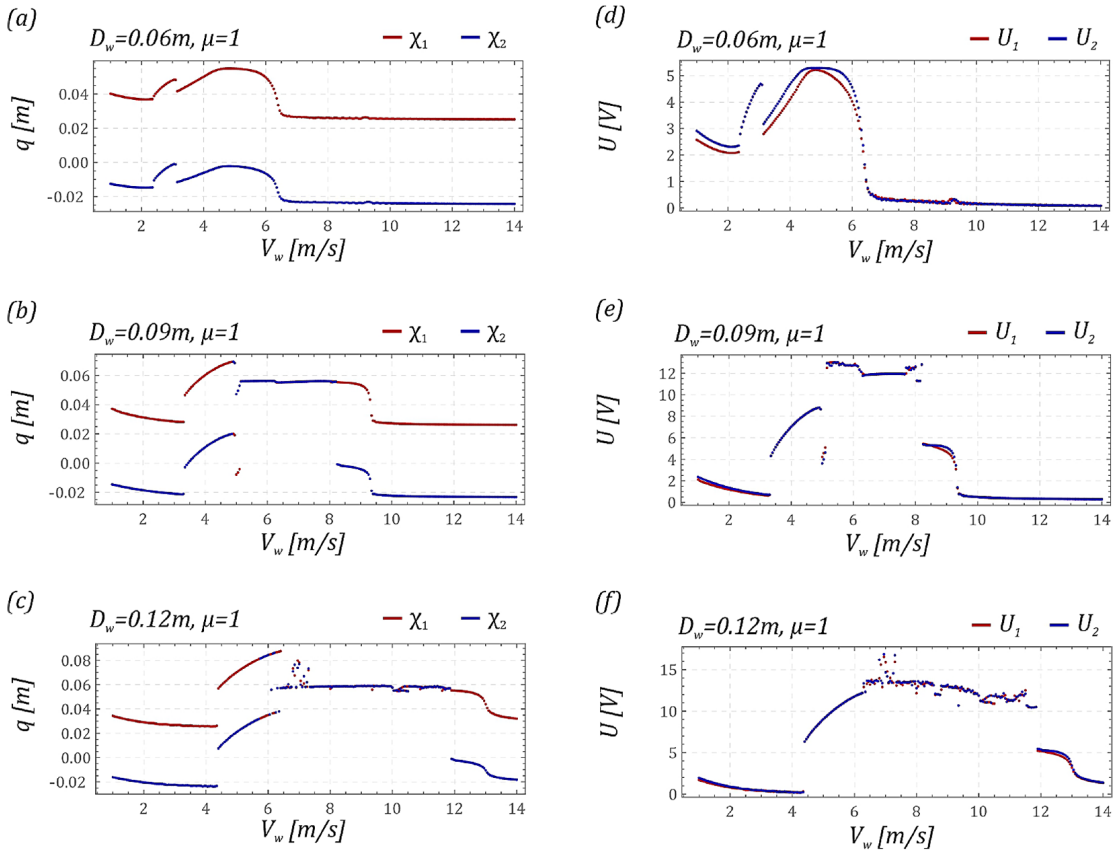

Figure 2. Output displacement and voltage (amplitudes) for increasing cylinder diameters D_w as a function of wind speed V_W: repulsive magnet configuration and dimensionless mass ratio μ = 1

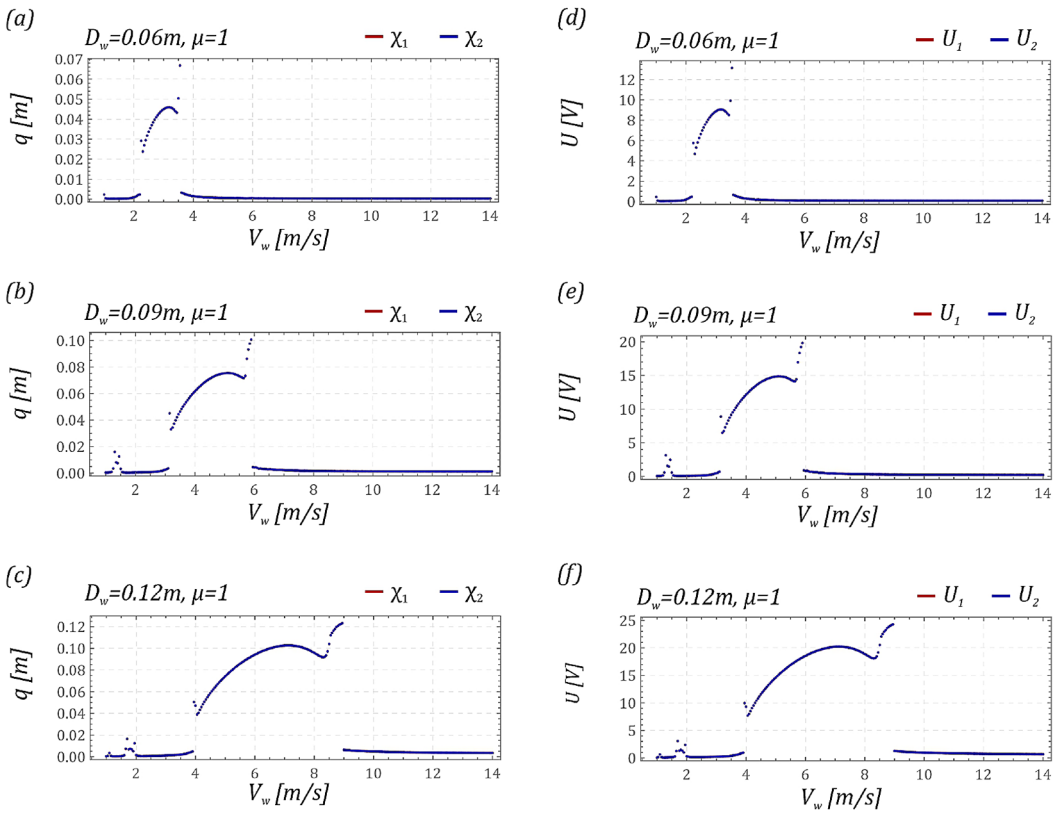

Figure 3. Output displacement and voltage (amplitudes) for increasing cylinder diameters D_W as a function of wind speed V_W: attractive magnet configuration and dimensionless mass ratio $\mu = 1$

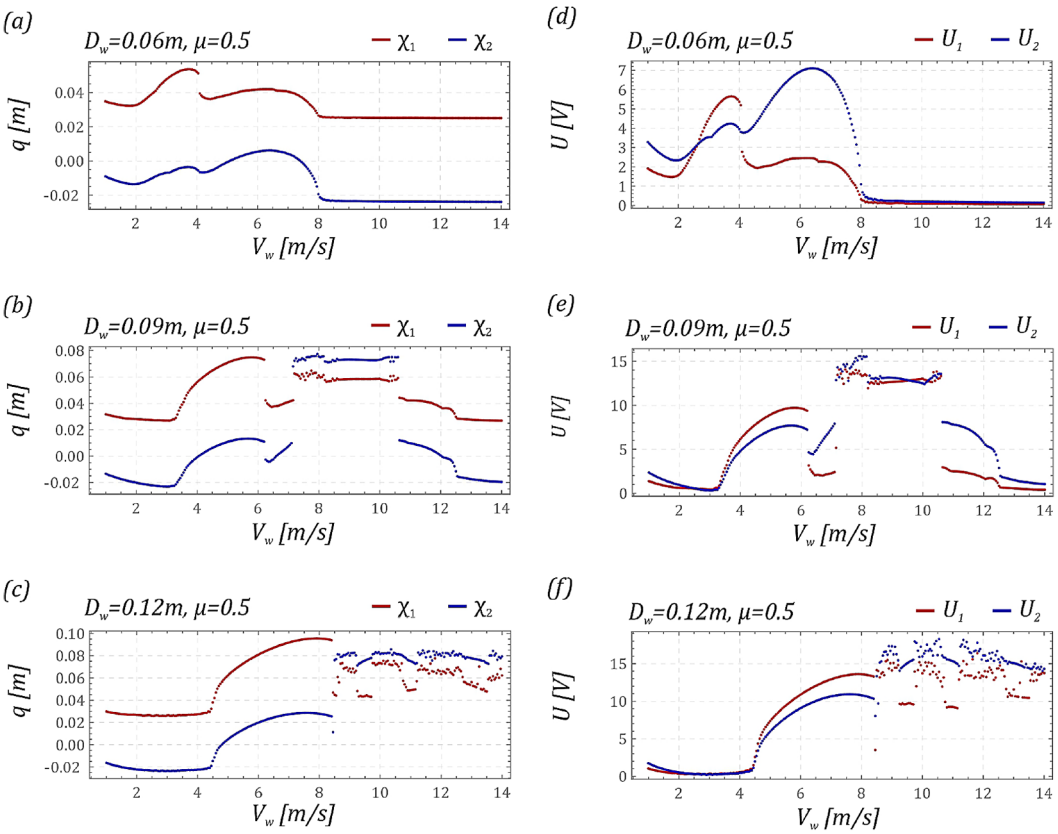

Figure 4. Output displacement and voltage (amplitudes) for increasing cylinder diameters D_W as a function of wind speed V_W: repulsive magnet configuration and dimensionless mass ratio $\mu = 0.5$

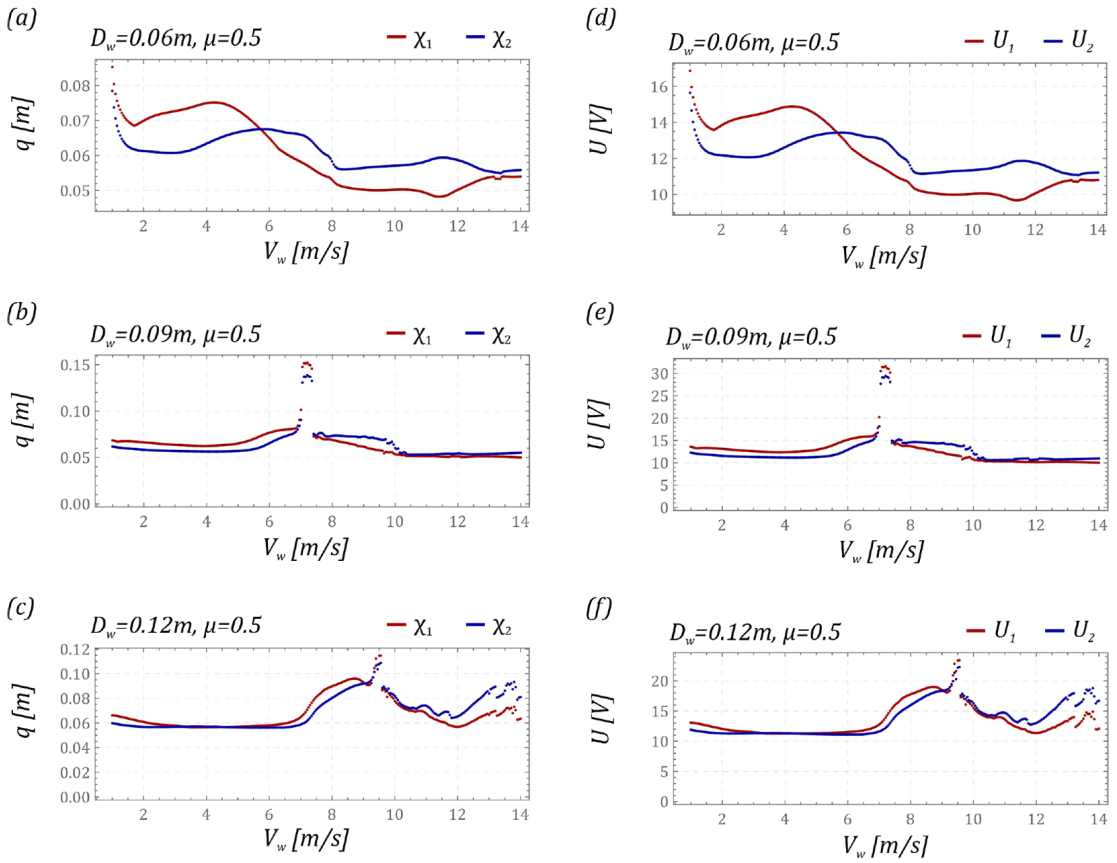

Figure 5. Output displacement and voltage (amplitudes) for increasing cylinder diameters D_W as a function of wind speed V_W: attractive magnet configuration and dimensionless mass ratio $\mu = 0.5$

velocities is associated with the nonlinear interaction between the vortices, the airflow, and the mechanical resonator.

Figures 2, 3, 4, and 5 present the displacement characteristics and the amplitudes of the voltages generated on the piezoelectric electrodes for various magnetic configurations. In the analyzed repulsive magnet configuration, it was observed that for a cylinder diameter of 0.06 m, the initially excited beam induces a motion counterphase to the second magnetically coupled beam. The highest voltages are generated within a flow velocity range of 3 to 6 m/s, while the device's broadband sensitivity spans from 1 to 6 m/s. Increasing the cylinder diameter to 0.09 m and 0.12 m leads to higher voltage outputs. For a diameter of 0.09 m, the maximum voltage reaches ~12 V in the 6–8 m/s range. For the 0.12 m diameter, the broadband response extends from 4 to 12 m/s, with an average voltage value close to 12 V. In the attractive magnet configuration, both beams operate synchronously. In this setup, the beam displacements are correlated, and the system response across the investigated diameter range (0.06–0.12 m) exhibits similar characteristics; however, the broadband efficiency is lower than that of the repulsive systems. A different characteristic is presented in Figures 4 and 5, where the system was analyzed with a mass ratio of $\mu = 0.5$ (the mass of the second beam being reduced relative to the first). In this configuration, a significant broadening of the operating range was observed in all cases. The best results were achieved for the 0.12 m diameter cylinder, where the operating bandwidth covers the range of 4–14 m/s, with a generated voltage of approximately ~16 V. A further increase in efficiency was recorded by simultaneously applying the attractive configuration and the mass ratio of $\mu = 0.5$. This combination resulted in the widest operating bandwidth, spanning from 1 to 14 m/s, and a nearly constant voltage output within the range of 15–20 V.

The analysis of the magnetic configurations reveals a significant impact on the synchronization and threshold behaviour of the system. In the attractive configuration with $\mu = 1$ (Fig. 3), a strong phase synchronization between the beams is observed, resulting in high voltage peaks within well-defined, yet narrower, synchronization zones. Conversely, the configuration featuring attractive

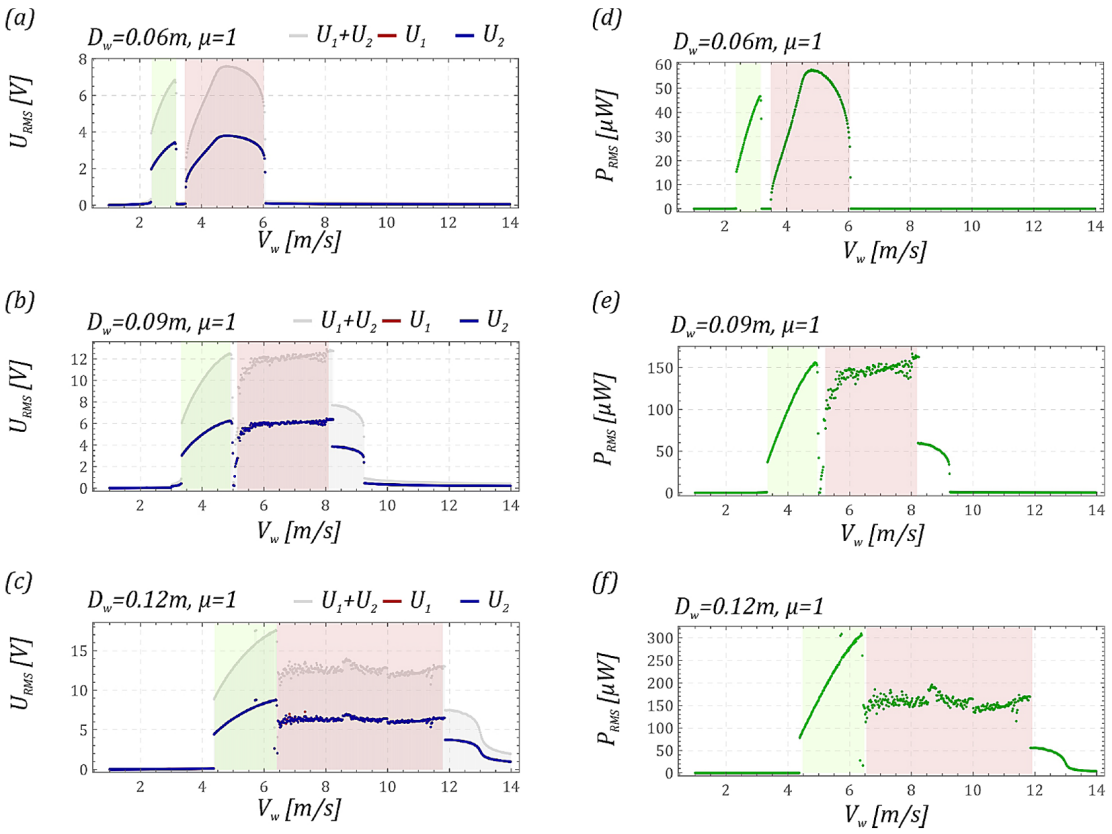

Figure 6. The RMS voltage output and RMS power for increasing diameter D_W of the cylinders as a function of the wind speed V_w: magnets repel and nondimensional mass ratio μ = 1

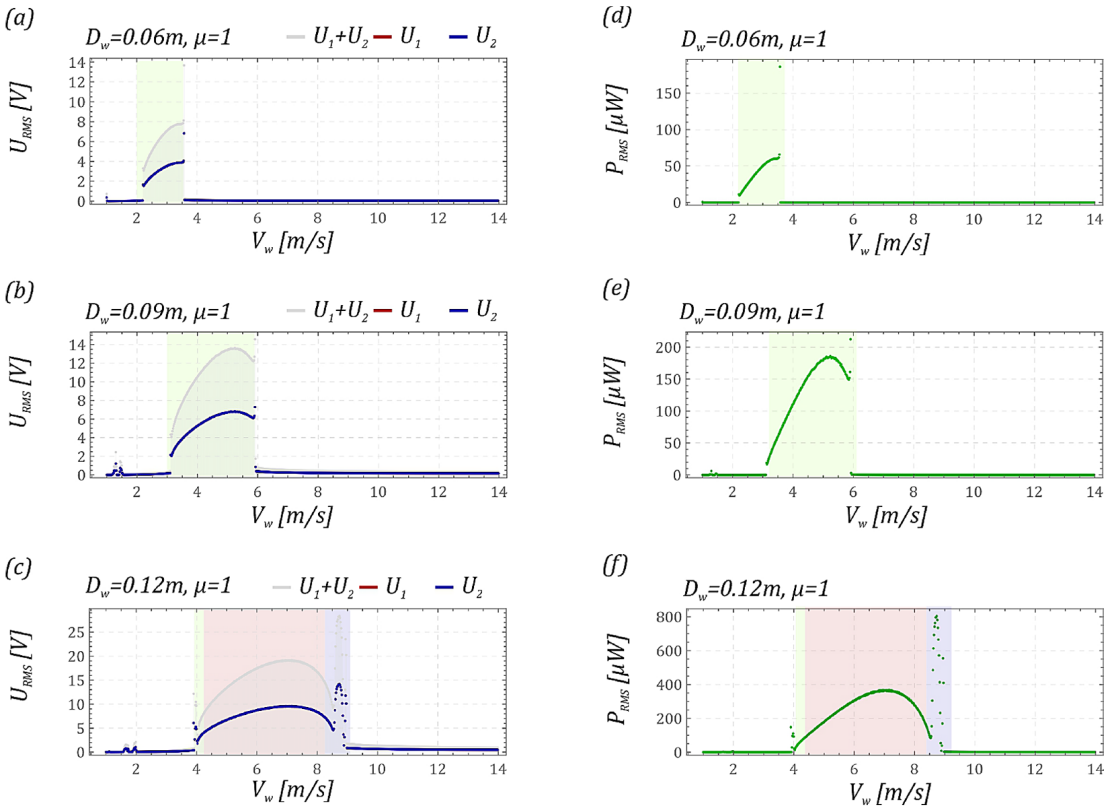

Figure 7. RMS voltage output and RMS power for increasing cylinder diameters D_W as a function of wind speed V_W: attractive magnet configuration and dimensionless mass ratio μ = 1

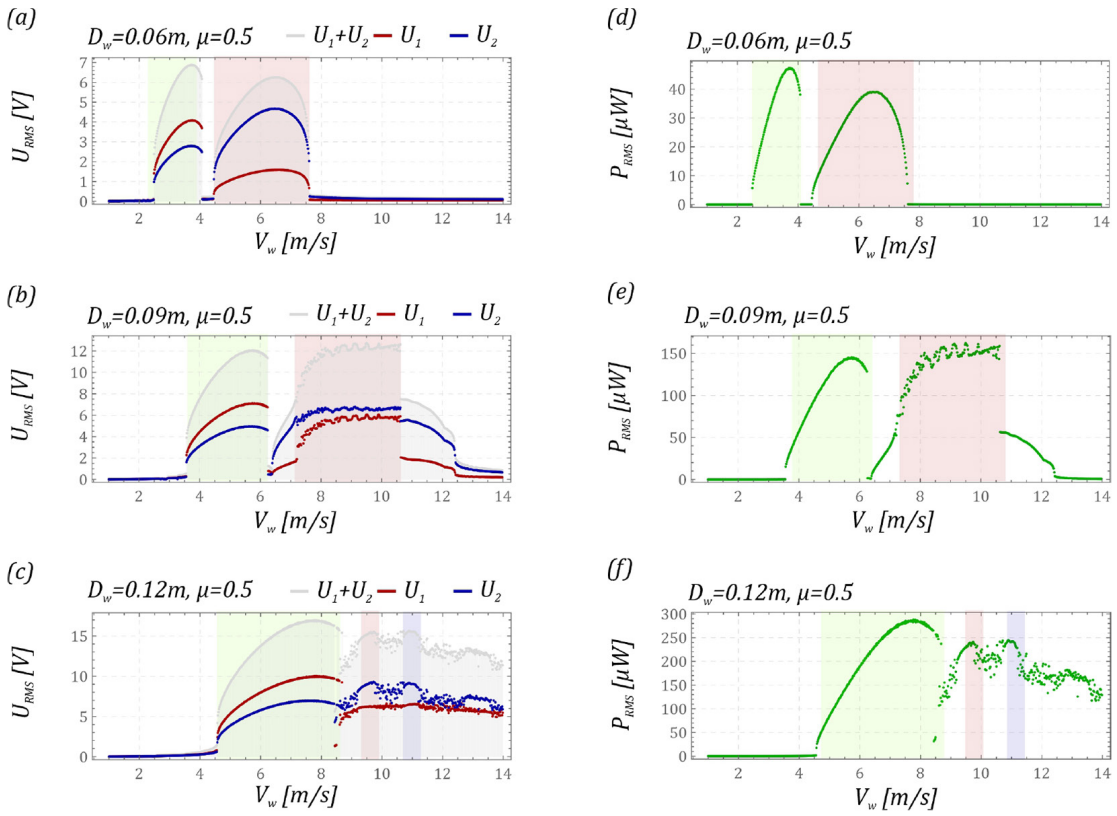

Figure 8. RMS voltage output and RMS power for increasing cylinder diameters D_W as a function of wind speed V_W: repulsive magnet configuration and dimensionless mass ratio $\mu = 0.5$

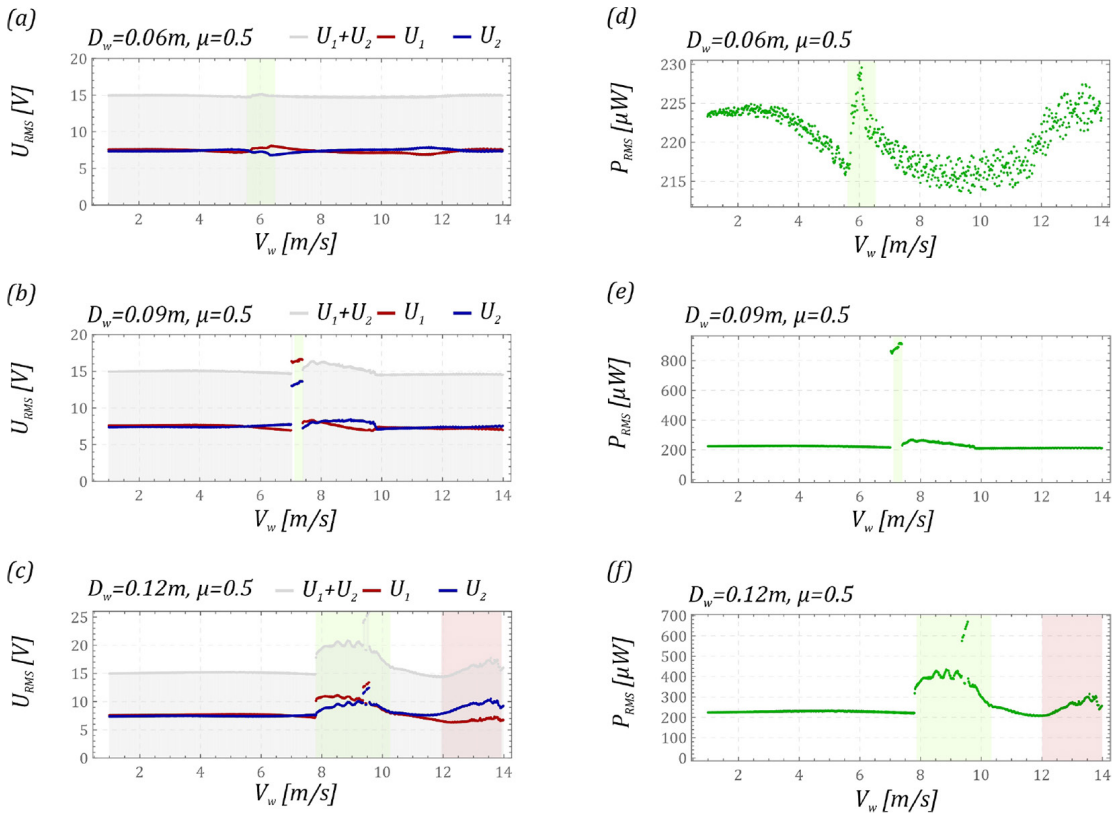

Figure 9. RMS voltage output and RMS power for increasing cylinder diameters D_W as a function of wind speed V_W: attractive magnet configuration and dimensionless mass ratio $\mu = 0.5$

magnets and a reduced mass ratio $\mu = 0.5$ (Fig. 5) demonstrates a superior aerodynamic performance by drastically lowering the cut-in wind speed. This combined effect allows the system to initiate energy harvesting at velocities as low as 1 m/s, providing a nearly continuous and stable power output across the entire investigated flow range. This suggests that system detuning via mass reduction, coupled with attractive magnetic forces, is a highly effective strategy for enhancing broadband energy harvesting in low velocities of wind.

Figures 6–9 present the root-mean-square (RMS) voltage values and the RMS power generated in various configurations. The system with a cylinder diameter of 0.12 m and $\mu = 0.5$ achieved a maximum power output of up to 700 μW (Fig. 9) in the attractive configuration. Analogous configurations with μ = 1 and attractive magnets reached up to 800 μW, albeit within a significantly narrower flow range (~8.5 m/s) (Fig. 7). The rapid transitions in the RMS voltage curves suggest the presence of bistable behavior, which is typical for systems with nonlinear magnetic interactions. Repulsive magnet configurations with a cylinder diameter of 0.06 m achieved RMS voltages of up to 8 V and a power level of 60 μW within the 2–3 m/s and 4–6 m/s ranges (Fig. 6). The widest operating range, combined with a high voltage output (averaging ~15 V), was recorded for the 0.12 m diameter cylinder in the configuration with μ = 1, where the operating bandwidth spanned 4–12 m/s with a generated power of approximately 200 μW (Fig. 6). For the same cylinder diameter and a mass ratio of μ = 0.5, the power reached 250 μW over an even broader flow range (Fig. 8).

CONCLUSIONS

The conducted analysis demonstrated that the application of two magnetically coupled beams constitutes an effective solution for broadening the bandwidth of efficient energy harvesting. Both the type of magnetic coupling (repulsive or attractive interaction of the magnetic poles) and the mass ratio μ significantly influence the system's characteristics.The best results were achieved for cylinders with diameters of 0.09 m and 0.12 m in configurations with attractive magnets. In particular, the configuration with a mass ratio of μ – 0.5 and a cylinder diameter of 0.12 m achieved maximum RMS voltages of up to 25 V and power levels of approximately 800 μW, while maintaining a wide operational excitation range from 1 to 14 m/s. These parameters underscore the high potential of the proposed designs for applications in flow-based energy harvesting systems. A notable enlargement of the low-velocity operational band was achieved via the coalescence of two separate resonance bands, driven by their close proximity. In addition, the inherent nonlinear coupling gave rise to a mutual synchronization effect, which promoted efficient energy transfer and absorption. The next step of this research will focus on the impact of geometric uncertainties of the magnetic elements and the numerical modeling of magnetic forces using the Finite Element Method (FEM). Additionally, incorporating relatively large cylinder masses on thin flexible beams inevitably introduces high dynamic stress concentrations at the mounting locations (beam roots). While this study focuses on aerodynamic energy conversion efficiency, evaluating the static strength, localized stress fields, and mechanical fatigue life of the piezoelectric cantilevers is a critical requirement for long-term operational reliability and will be thoroughly investigated in future works. In terms of practical deployment, the proposed broadband harvester is ideally suited for powering low-power, self-sustained components within industrial and transport infrastructure. Specific applications include wireless structural health monitoring on bridges, real-time leakage and pressure monitoring nodes along remote pipelines, and localized environmental telemetry sensors where battery replacement is unjustified.

Acknowledgement

This research was funded by the National Science Centre, Poland under the OPUS call in the Weave programme under the project no. 2023/51/I/ST8/02739.

REFERENCES

1. Ahmed, M.M,. Dipu, N.Z., Badhon, M.A., Md. Mahbub Alam, M.M., Cheng, T., Masud, M.H. (2026). Piezoelectric harvestersfor flow-induced vibration energy: recent advances, challenges, and prospects, *Int. J, Ener. Resear.,* 2566605. https://doi.org/10.1155/er/2566605
2. Borowiec, M., Bocheński, M., Drzymała, B., Ostrowski, M. (2026). Analysis of an energy harvesting system with kinematic excitation and step change

of elastic force with hysteresis. *Advances in Science and Technology Research Journal*, *20*(3), 512–524. https://doi.org/10.12913/22998624/213964

3. Cottone, F., Vocca, H., Gammaitoni, L. (2009) Nonlinear energy harvesting. *Phys. Rev. Lett. 102*, 080601. (2009)
4. Erturk, A., Hoffmann, J., Inman, D.J. (2009). A piezomagnetoelastic structure for broadband vibration energy harvesting *Appl. Phys. Lett*., *94*, 254102.
5. Facchinetti, M.L., De Langre, E., Biolley, F. (2004). Coupling of structure and wake oscillators in vortex-induced vibrations. *J. Fluids Struc*., *18,* 123–140.
6. Gazkooh, H.K., Sadhu, A., Liu, K. (2025). Vibration-based energy harvesting in largescale civil infrastructure: a comprehensive outlook of current technologies and future prospects, Discover Civil Engineering, *2*, 154. https://doi.org/10.1007/s44290-025-00308-7
7. Jing G., Zhang, R., Connolly, D.P., Hou, W., Aela P. (2025), Piezoelectric energy harvesters for railways: recent trends and future opportunities, Multiscale and Multidisciplinary Modeling, *Experiments and Design*, *8*, 325. https://doi.org/10.1007/s41939-025-00919-8
8. Litak G., Caban J., Sadasiavan S., Klimek M., Margielewicz J., Gąska D. (2025). Wind induced energy harvesting with an aero-elastic resonator: Effect of the bluff body diameter. *J. Ecol. Eng.*, *26*, 197–204.
9. Litak, G., Friswell, M.I., Adhikari, S. (2010). Magnetopiezoelastic energy harvesting driven by random excitations. *Applied Physics Letters*, *96*, 214103.
10. Liu, C., Zhang, B., Dong, L., Zhong, J., Wang, J., Wang, Y. (2026). A review of energy harvesting techniques based on flow-induced vibrations, *Applied Energy*, *416* 127937.
11. Ma, X., Zhang, H., Margielewicz, J., Gąska, D., Wolszczak, P., Litak, G., Zhou, S. (2024). A dual-beam piezo-magneto-elastic wake-induced vibration energy harvesting system for high-performance wind energy harvesting, Science China Technological Sciences, *67*, 221–239.
12. Ma, X., Zhou, S. (2022). A review of flow-induced vibration energy harvesters. *Ener. Conv. Manag*., *254*, 115223.
13. Maity, S., Ali, S.F., Litak, G. (2026). Performance enhancement of a coupled magneto-mechanical harvester through impact. *Chaos, 36*, 073139.
14. Maity, S., Litak, G., Ali, S.F. (2026). Energy transfer, multistability, and chaos in coupled vortex-induced vibration harvesters: a semi-analytical approach. *Nonlinear Dynamics*, *114,* 1098.
15. Margielewicz, J., Gąska, D., Litak, G., Wolszczak, P., Yurchenko, D. (2022). Nonlinear dynamics of a new energy harvesting system with quasi-zero stiffness *Applied Energy*, *307,* 118159.
16. Sadasivan, S., Litak, G., Furquan, M., John, B., Gęca, M,J. (2025). Computational investigation of vortex-induced oscillation of two side-by-side cylinders at high Reynolds numbers. *European Journal of Mechanics-B/Fluids*, *110*, 1–18.
17. Sang, J.Y., Wu, Y.Z., Zeng, Z.T., Kong, D.B., Liu, H.P., Wang, G.Q. (2026) Synergetic enhancement of bi-stable piezoelectric energy harvester using in-plane lateral constraint and magnet-spring oscillator. *Applied Physics A-Materials Science & Processing*, *132*, 206.
18. Shehu, L., Yeon, J.H., Song, Y. (2024). Piezoelectric energy harvesting for civil engineering applications. *Energies*, *17*, 4935. https://doi.org/10.3390/en17194935
19. Su, B., Guo, T., Alam, M.M. (2025). A review of wind energy harvesting technology: Civil engineering resource, theory, optimization, and application, *Applied Energy*, *389*, 125771.
20. Ullah, Q., Rauta, T., Keskikuru, J., Haverinen, J., Ruuskanen, P. (2025). Innovations in energy harvesting: A survey of low-power technologies and their potential. *Energy Reports*, *14*, 671–692.
21. Wang, J., Gu, S., Zhang, C., Hu, G., Chen, G., Lai, Y., Yang, K., Li, H., Litak, G., Yurchenko, D. (2020). Hybrid wind energy scavenging by coupling vortex-induced vibrations and galloping, *Ener. Conv. Manag.*, *213*, 112835.
22. Yang, T., Zhou, S., Litak, G., Jing, X. 2023. Recent advances in correlation and integration between vibration control, energy harvesting and monitoring. Nonlinear Dynamics, *111*, 20525–20562.
23. Yang, Z., Zhou, S., Zu, J., Inman, D. (2018). High-performance piezoelectric energy harvesters and their applications. *Joule*, *2*, 642-697.
24. Zhang, Y., Li, S., Wang, W., Zen, P., Li, C., Ye, Y., He, X. (2025). A Review of Electromagnetic Wind Energy Harvesters Based on Flow-Induced Vibrations, *Energies*, *18,* 3835. https://doi.org/10.3390/en18143835
25. Zhou, Y., Lu, P., Zhou, X., Bai, J., An, S., Liu, S., Pu, X. (2024). Triboelectric wind sensors: Fundamentals, progress, and perspective. *Nano Energy Part A*, *131*, 110209. https://doi.org/10.1016/j.nanoen.2024.110209
26. Zhang, Y., Wang L., Lei, Y., Wang, W., Bowen, C., Xu, Y. Bader S., Arafa, M., Cao J., Liao, W-H. (2026). A review on energy harvesting for sustainable IoT monitoring systems, *Renewable and Sustainable Energy Reviews*, *232*, 116779.